Applied Physics B (2024) 130:157
https://doi.org/10.1007/s00340-024-08294-x

Applied Physics B
Lasers and Optics

RESEARCH

Enhanced emission in the NIR range by Nd^{3+} doped borosilicate glass for lasing applications

Yasha Tayal[1] · Rupesh A. Talewar[2] · Sk. Mahamuda[3] · Kartika Maheshwari[1] · Sheetal Kumari[4] · Mohit Kumar[4] · Ravita Pilania[5] · Aman Prasad[6] · A. S. Rao[4]

Received: 4 April 2024 / Accepted: 26 July 2024 / Published online: 12 August 2024

Abstract
Borosilicate glasses were prepared via melt quench technique with different concentration of Nd^{3+} ions. X-ray diffraction (XRD) was performed for the prepared glass to study the amorphous structure. The glass stability was studied by Thermogravimetric Analysis (TGA). Spectroscopic analysis of the prepared glasses was done through absorption, excitation, emission and decay measurements. Absorption spectra was used to evaluate the J-O parameters. Radiative parameters are evaluated with the help of application of J-O theory. Emission spectra show three prominent bands in NIR region arising from $^4F_{3/2} \rightarrow {}^4I_{9/2}$, $^4I_{11/2}$ and $^4I_{13/2}$ centered around 910, 1068 and 1339 nm accordingly, with the most intense being the one at 1068 nm. Stimulated emission cross section, branching ratio and quantum efficiency for $^4F_{3/2} \rightarrow {}^4I_{11/2}$ transition is very high and is suitable for lasing applications. Dipole–dipole interaction is observed among activator ions on the basis of Dexter theory. The optimized Nd^{3+} doped glass (NBS10) possess maximum value for all radiative parameters and hence can be best suited for applications in the area of lasers and fiber amplifiers.

1 Introduction

Hyaline substances doped with a rare earth (RE) ions find vast usage in numerous optoelectronic devices like light emitting diodes (LEDs), fiber amplifiers, solid state lasers, optical waveguides, temperature sensors, etc. [1–5]. Intense lasing emissions in NIR range for Nd^{3+} places it as most famous RE ion for luminescence based characteristics [6, 7]. The transition at 1068 nm is sharpest and hence, is vastly explored for usage in high power lasers. Also, it can be observed easily at room temperature [8, 9]. While the one associated with 1340 nm finds huge utility in enhancing the O-band optical signal and provides a window in telecommunication transition, the emission centered around 900 nm provides a window for forging a device that could produce blue emission via monolithic integration of emission from a powerful diode laser [10, 11].

Various glassy systems like silicate, borates, phosphates, tellurites, chalcogenides and fluorides have been explored for the NIR range luminescence via Nd^{3+} ions [7, 10, 12–15]. Among these, borosilicate, a combination of borate and silicate glass systems, provides fine RE ion solubility, good mechanical strength, thermal and chemical durability [16]. Further, luminescence characteristics can be enhanced by reducing the phonon energy in the glass host, which in turn produces further utility for fiber amplifiers and high efficiency lasers [16, 17]. Phonon energy in this system can be lowered upon introduction of heavy metal oxide (PbO) which also increases the refractive index for the glass system. It further helps in reduction of transition temperature and allows for a wider spectral transmission window. Incorporation of ZnO, a non-toxic and non-hygroscopic oxide in the host matrix paves the way for better optical, magnetic and electrical characteristics.

✉ Yasha Tayal
yashaphy10nov@gmail.com

1 ABES Engineering College, Ghaziabad 201009, India

2 Physics Department, Shri Ramdeobaba College of Engineering and Management, Katol Road, Nagpur 440013, India

3 Department of Engineering Physics, College of Engineering, Koneru Lakshmaiah Education Foundation, Vaddeswaram 522302, India

4 Department of Applied Physics, Delhi Technological University, Bawana Road, New Delhi 110042, India

5 Department of Physics, Chaudhary Bansilal University, Bhiwani 127021, India

6 Department of Physics and Computer Science, Dayalbagh Educational Institute (DEI), Deemed University, Agra 282005, India

ZnO also possess some unique properties like direct wide band gap, large intrinsic emitting and higher exciting binding energy which in turn helps the glass system to find applications in solar energy converters, optoelectronic devices and gas sensors. By taking up the tetrahedral and octahedral positions in the host matrix, the addition of Al_2O_3 enhances its chemical and thermal stability as well as its mechanical strength, emission characteristics, and solubility of RE ions. It also decreases crystallization. The inclusion of alkali oxides (Li_2O, Na_2O, etc.) in the borate matrix can change the three coordinated boron atoms in the system into four coordinated tetrahedral structure, which improves chemical stability and causes non-bridging oxygens (NBO) to be produced [18–22]. As compared to phosphors, glasses possess easier fabricating technique and lower melting temperature leading to better incorporation in the optical devices [10, 23].

Nd^{3+} ions populate the $^4F_{5/2}$ level via pumping and later decay to $^4F_{3/2}$ state via non-radiative transition (multi phonon relaxation). Subsequently, the ions decay to $^4I_{13/2}$, $^4I_{11/2}$ and $^4I_{9/2}$ levels from $^4F_{3/2}$ emitting radiation in NIR range at 900, 1068 and 1340 nm respectively. These NIR range emissions have two major setbacks. Firstly, nearby Nd^{3+} ions tend to suffer cross relaxation mechanism, leading to quenching thereby mandating an optimized concentration of Nd^{3+} ions [24, 25]. Secondly, to acquire a rapid multi phonon relaxation rate of Nd^{3+} ions from the $^4F_{5/2}$ ($^2H_{9/2}$) to $^4F_{3/2}$ level when excited by 585 nm, the ambient phonon energy possessed by glass host should be close to the bridge energy gap (~1000 cm^{-1}). Minimum non radiative transition produced by multiphonon relaxation provides a good window for quantum yield and hence can be better used as laser amplifiers.

Great interest by numerous researchers has been observed in studying the physical, absorption and fluorescence properties of Nd^{3+} doped glass matrix and it can be improvised by selecting appropriate glassy system [26–28]. In the present study, we aim to prepare Nd^{3+} ions doped borosilicate glass and hence to identify the improvised NIR lasing band obtained upon the introduction of optimized Nd^{3+} content. On account of above scientific parameters, we prepared a borosilicate glass with Li_2O, PbO, ZnO and Al_2O_3 as intermediates for enhanced thermal and mechanical strength. Dwelling upon the aforementioned utilities, we intend to state a pertinent examination of lithium lead zinc alumino borosilicate glass doped via various concentrations of Nd^{3+} ions figuring out optimized content of the RE ion for intense laser emission at 1068 nm.

2 Experimental procedure

With the help of melt quench technique Nd^{3+} doped glasses were prepared according to the following glass composition: $10Li_2O–5PbO–(5–x)ZnO–10Al_2O_3–10SiO_2–60B_2O_3–xNd_2O_3$, where, $x = 0.1$, 0.5, 1.0, 1.5, 2.0 and 2.5 mol%. For the ease of recognition, these samples were tagged as NBS01, NBS05, NBS10, NBS15, NBS20 and NBS25 accordingly. The starting reagents i.e. H_3BO_3, SiO_2, PbO, ZnO, Al_2O_3, Li_2O and Nd_2O_3 of high purity (98–99.99%) were taken. A batch of 7.0 g of ingredient chemicals were measured and then grounded finely via agate mortar so as to obtain homogeneous mixture. This mixture was transferred to an alumina crucible and then placed in an electric furnace at 1100 °C for 3 h. The melt so obtained was suddenly quenched by decanting it on a preheated brass plate and pressing with a similar one. The obtained glass samples were further annealed in a muffle furnace at 350 °C for about 4 h. This process helps in releasing internal mechanical stress which avoids cracking and bubbles formation in the glass samples. Figure 1 shows the photograph of Nd^{3+} ions doped NBS glasses. These samples were then characterized at room temperature (RT). Archimedes' principle and Brewster's method was used to estimate the densities and refractive indices respectively of NBS glasses using xylene as the immersion liquid. Using an XPERT-PRO diffractometer, the XRD spectral recordings were made with a step size of 0.02 and a 2θ angle that ranged from 10° to 75°. JASCO V-670 model UV–vis–NIR spectrophotometer was used to record the optical absorption spectra of the samples. Hitachi-F7000 fluorescence

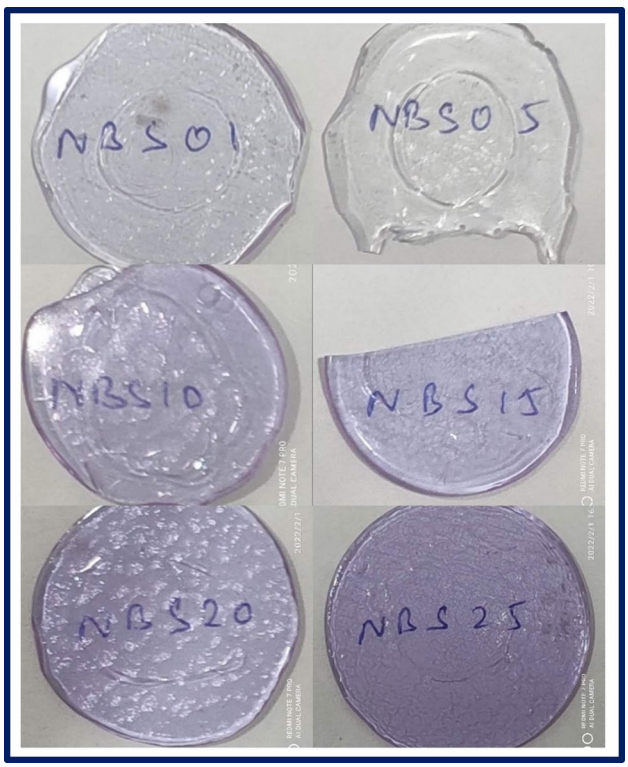

Fig. 1 Nd^{3+} ions doped NBS glass samples

spectrofluorometer was used to record photoluminescence (PL) excitation, emission spectra and fluorescence decay.

3 Results and discussion

3.1 Physical properties and XRD

Density is a useful tool for examining changes in coordination, the degree of structural compactness, the geometrical topologies of the glass network, and the dimensions of interstitial holes. The values of density measured for the present glass system are 2.64, 2.66, 2.67, 2.69, 2.73 and 2.76 g/cm^3 as the mol% of Nd^{3+} ions increased from 0.1 to 2.5 mol% respectively. The refractive index of optical materials is another crucial parameter. The values of refractive index measured for the 0.1 to 2.5 mol% of Nd^{3+} ions doped NBS glasses are 2.42, 2.47, 2.51, 2.54, 2.59 and 2.62 respectively. The calculated values of molar volume for the 0.1 to 2.5 mol% of Nd^{3+} ions doped NBS glasses are 3062, 3077, 3114, 3138, 3139 and 3151 cm^3 respectively. Figure 2 shows that the refractive index, density and molar volume of the glasses which increase as the concentration of Nd^{3+} ions rises, signifying the addition of Nd_2O_3 in place of B_2O_3. These increasing values of density and molar volume suggest that there are more non-bridging oxygen molecules (NBOs) in the glass network. Since Nd_2O_3 enters the glass network as a network modifier, occupies an interstitial space within the network and ultimately produces NBOs in the glass structure, the glass network grows with the addition of Nd_2O_3.

Figure 3 depicts the XRD pattern of the un-doped NBS glass. It shows the amorphous behaviour of the as-synthesized glass. The broad hump signifies absence of long range order in the glass lattice.

3.2 Thermal analysis

The TGA curve was utilized to calculate the weight loss and identify the weight loss mechanisms of the powder precursors to form pure NBS glass. As seen in Fig. 4, the TGA curve illustrates weight loss across three separate stages

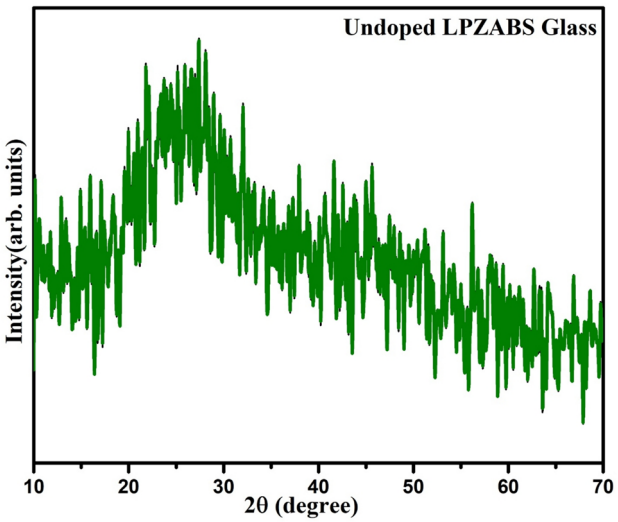

Fig. 3 XRD pattern of undoped NBS glass

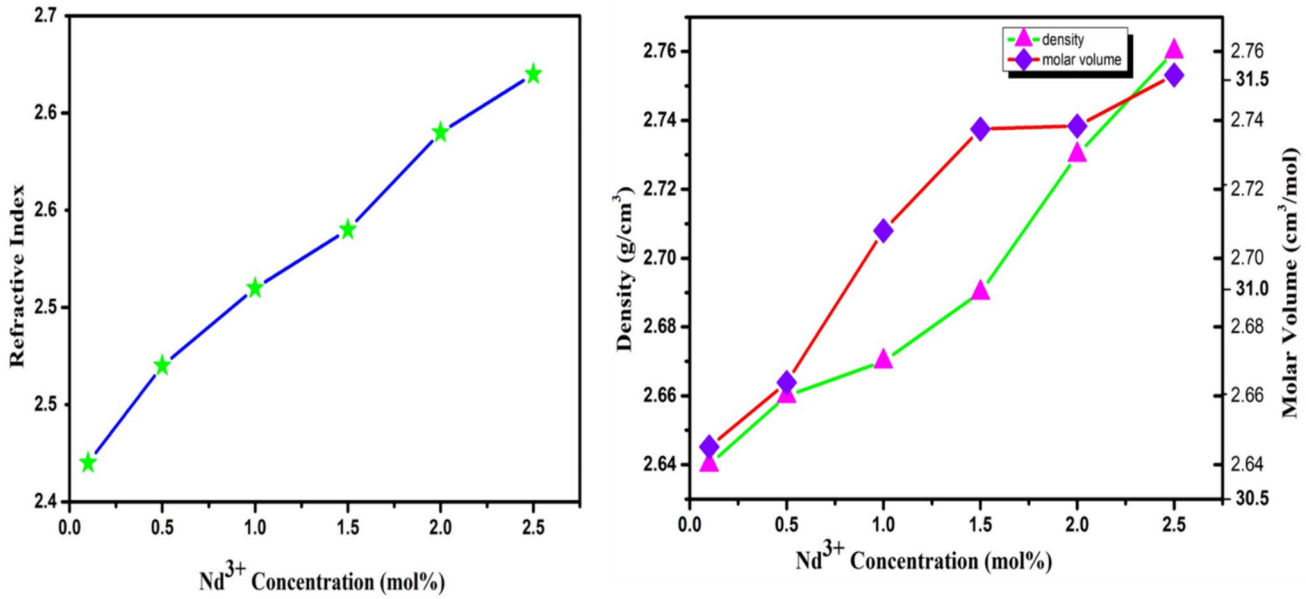

Fig. 2 Variation of refractive index, density and molar volume with the concentration of Nd^{3+} ions in NBS glass samples

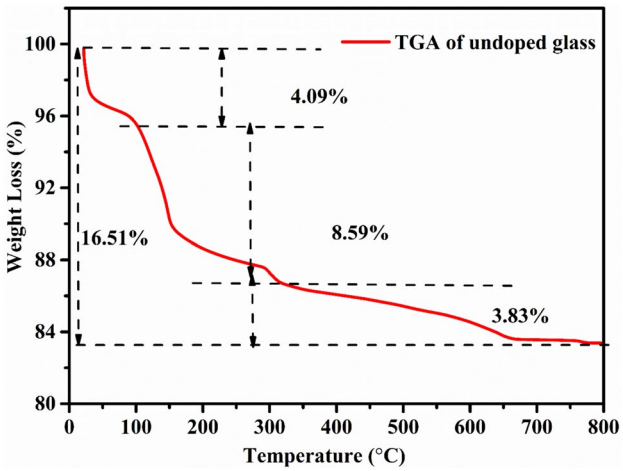

Fig. 4 TGA curve for the undoped sample

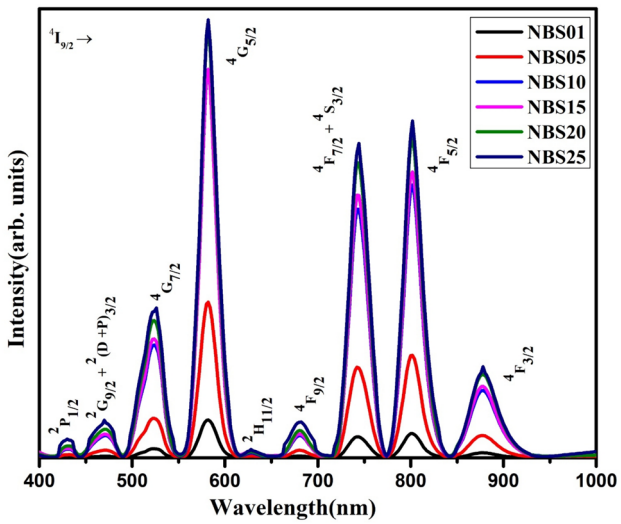

Fig. 5 Absorption spectra of Nd^{3+} ions in NBS glasses

from 21 to 800 °C. Evaporation of the absorbed water from the sample's surface causes a weight loss of 4.09% during the first stage, which is observed between 21 and 102 °C. The exhaustion and breakdown of remaining oxides in the sample is represented by the second stage (102–334 °C), which has a weight loss of 8.59%. The presence of combustibles in the sample is the reason of the third stage, which is between 334 and 768 °C and has a weight loss of 3.83%. The evaporation of various gases and the exhaustion of organic species cause a total weight loss of around 16.51%. Therefore, it is evident from Fig. 4 that the glass sample have a lesser mass loss at high temperatures and is thermally more stable.

3.3 Absorption spectrum and Judd–Ofelt parameters

Absorption spectra for Nd^{3+} doped NBS glass is shown in Fig. 5 for the wavelength range of 300–1100 nm. The figure comprises of various peaks of f–f electronic transitions belonging to Nd^{3+} ions from their ground state. The transitions found in the UV–vis–NIR range are from $^4I_{9/2} \rightarrow {}^4F_{3/2}$, $^4F_{5/2}$, $^4F_{7/2} + {}^4S_{3/2}$, $^4F_{9/2}$, $^2H_{11/2}$, $^4G_{5/2}$, $^4G_{7/2}$, $^4G_{9/2} + {}^2(D+P)_{3/2}$ and $^2P_{1/2}$ which are centered at 876, 800, 743, 680, 628, 582, 525, 470 and 429 nm respectively. These transitions are quite identical to other reported Nd^{3+} doped glasses excluding the minor changes in band positions and respective intensities, on account of the present glass system possessing diverse ligand fields having corresponding nature [7, 29]. As the intensity for all bands increases on increasing the Nd^{3+} content in the glass, it can be concluded that the Nd^{3+} ions are very well homogeneously dissolved in the glass matrix.

Nephelauxetic ratio (β) and bonding parameter (δ%) help in determination of the type of Nd^{3+} ligand bond [16].

$$\beta = \frac{\Upsilon_a}{\Upsilon_b} * 100 \tag{1}$$

here, Υ_a, Υ_b represents the energies for the transitions in complex and free ion or aqua ion respectively as given in Carnall paper [30]. From all calculated β values respective to the transitions occurring in absorption spectra, $\bar{\beta}$ the average value was calculated, which further helps in determination of the bonding parameters by using following expression:

$$\delta\% = \left[\frac{1-\bar{\beta}}{\bar{\beta}}\right] \times 100 \tag{2}$$

Bonding parameter value is either positive or negative corresponding to covalent or ionic bonding of the RE ions with the local host in glassy system. Hence, as the values obtained for the bonding parameters are positive for all Nd^{3+} doped NBS glasses, we can conclude that the bonding between the ions is covalent in nature. The values of nephelauxetic ratios and bonding parameters of all the samples are tabulated in Table 1.

Various important parameters like experimental oscillator strength, Judd–Ofelt parameters, various radiative properties such as transition probability, radiative lifetime and fluorescence branching ratio rely upon the data from the absorption spectra. The area under the curve for each transition occurring in absorption band is used to estimate the experimental oscillator strength (f_{exp}) of f–f induced electric -dipole transitions by the following expression [1, 8]:

$$f_{exp} = 4.32 \times 10^{-9} \int_{\nu 1}^{\nu 2} \varepsilon(\nu) d\nu \tag{3}$$

Table 1 Experimental (f_{exp}) ($\times 10^{-6}$), calculated (f_{cal}) ($\times 10^{-6}$) oscillator strengths, r.m.s deviation (δ_{rms}), nephelauxetic ratio ($\bar{\beta}$) and bonding parameters (δ %) of Nd^{3+} ions in NBS glasses

Transitions $^4I_{9/2}\rightarrow$	NBS01		NBS05		NBS10		NBS15		NBS20		NBS25	
	f_{exp}	f_{cal}	f_{exp}	f_{cal}	f_{exp}	f_{cal}	f_{exp}	f_{cal}	f_{exp}	f_{cal}	f_{exp}	f_{cal}
$^4F_{3/2}$	3.32	2.72	3.81	2.92	4.07	3.13	2.82	2.41	2.37	2.03	1.97	1.76
$^4F_{5/2}$	11.94	12.52	12.04	13.15	14.91	15.98	10.34	11.35	8.74	9.61	7.28	8.01
$^4F_{7/2}+{}^4S_{3/2}$	10.74	9.98	11.75	10.42	14.44	13.11	10.27	9.12	8.69	7.72	7.17	6.37
$^4F_{9/2}$	0.92	1.45	0.93	1.52	1.06	1.89	0.95	1.32	0.85	1.12	0.74	.92
$^2H_{11/2}$	0.18	.39	0.19	.41	0.20	.50	0.13	.35	0.11	.30	0.10	.25
$^4G_{5/2}$	32.67	32.65	33.64	33.65	37.99	37.97	25.58	25.64	19.65	19.71	15.80	15.86
$^4G_{7/2}$	5.45	5.72	6.07	6.02	6.54	6.76	6.09	4.87	5.07	3.98	4.48	3.34
$^2G_{9/2}+{}^2(D+P)_{3/2}$	0.48	.54	1.04	.57	1.15	.65	0.99	.48	0.87	.40	0.63	.34
$^2P_{1/2}$	0.65	.42	0.91	.47	1.05	.42	0.79	.36	0.66	.31	0.61	.28
$\delta_{rms}(\times 10^{-6})$	0.439		0.715		0.768		0.720		0.617		0.555	
$\bar{\beta}$	0.9954		0.9955		0.9957		0.9958		0.9965		0.9969	
δ%	0.4591		0.4495		0.4239		0.4164		0.3504		0.3084	

Here, for the wavenumber (cm^{-1}), $\varepsilon(\nu)$ represents the molar extinction coefficient while $d\nu$ represents the half-bandwidth corresponding to the absorption band. If Gaussian shapes do occur for the absorption bands, then for such circumstances oscillator strength could be easily determined by half width technique according to the relation [1, 8]:

$$f_{exp} = 4.32 \times 10^{-9} \sum \Delta\nu \tag{4}$$

Here, $\Delta\nu$ (cm^{-1}) represents the width of the band at half the intensity of the peak. However Gaussian shape does not occur for glasses generally and bands suffer from inhomogeneous broadening which forces us to not use the latter technique, as it would give inaccurate results. For the present study, intensities for all absorption bands have been determined via area method. Calculated oscillator strength (f_{cal}) are evaluated in accordance with the Judd–Ofelt (J–O) theory, for f–f intensity model with the help of least square fit analysis from initial to final state [31]. Proper relation for estimating the f_{cal} was used from literature [32, 33]. Root mean square deviation (δ_{rms}) is used to estimate the goodness of fit among f_{exp} and f_{cal} by the equation:

$$\delta\text{rms} = \left[\frac{\sum \left(f_{exp} - f_{cal}\right)^2}{p}\right]^{1/2} \tag{5}$$

The number of energy levels in totality for present fitting technique are represented by p. The experimental and calculated oscillator strengths along with δ_{rms} are shown in Table 1 for all Nd^{3+} doped NBS glasses. Smaller values of δ_{rms} signifies the precision of estimation used. Applying least square fitting procedure provided in literature [34], the three J–O intensity parameters Ω_t (t = 2, 4, 6) for Nd^{3+} ions doped NBS glasses have been determined and are listed in Table 2 with other reported JO parameters [35–38]. The trend followed by JO parameters for Nd^{3+} doped NBS glasses is $\Omega_6 > \Omega_2 > \Omega_4$ and these values increase upto 1 mol%. Beyond this concentration, the values for these three parameters decrease. As similar dopant sites are occupied, the JO intensity characteristics ideally do not need to vary with concentration in the same host. However, if the clustering of dopant ions occurs, then variation in JO intensity parameters is observable, like the one noticed in the present work [39]. These three parameters are concerned with numerous physical and structural characteristics of glasses. Ω_2 is highly sensitive to the RE ions surroundings and is associated with the lack of symmetry with respect to coordination structure, type of bonding and polarizability of ligand ions. Since Ω_2 is correlated with the asymmetry of the immediate environment around the Nd^{3+} sites, it demonstrates the reliance of the covalence between Nd^{3+} ions and ligand anions. The ion site becomes less centro symmetrical and forms a stronger ionic chemical interaction with the ligands when the Ω_2 parameter values increase. The current investigation reveals that the values of Ω_2 changes from 5.8593 to 5.7406 and then increases to 6.4213 as the concentration of Nd^{3+} ions increases from 0.1, to 0.5 and to 1.0 mol%, respectively, indicating a rise in the covalent nature of the Nd–O bond. The values obtained in the present study are higher than the values reported in the different composition, presented in the Table 2 [35–38]. Ω_4 is the parameter which defines the bulk characteristics such as rigidity and viscosity of the host glass system comprising of the RE ions. Ω_6 is inversely proportional to the covalency of Nd–O bonds and this can be altered on modification of the host glass structure or composition [40, 41]. J-O intensity parameters for NBS10 glass shows the highest value among the six prepared glasses by varying Nd^{3+} ion content, so we can say that NBS10 possess

Table 2 Judd–Ofelt parameters ($\Omega_\lambda \times 10^{-20}$cm^2) and their spectroscopic quality factor ($\chi = \Omega_4/\Omega_6$) of Nd^{3+} ions in NBS glasses along with various reported hosts

Glass system	Ω_2	Ω_4	Ω_6	χ	Trend	References
NBS01	5.8593	1.6311	7.1709	0.227	$\Omega_6 > \Omega_2 > \Omega_4$	Present work
NBS05	5.7406	1.7295	7.1778	0.240	$\Omega_6 > \Omega_2 > \Omega_4$	Present work
NBS10	6.4213	1.4773	8.7806	0.168	$\Omega_6 > \Omega_2 > \Omega_4$	Present work
NBS15	4.0929	1.2659	5.9441	0.213	$\Omega_6 > \Omega_2 > \Omega_4$	Present work
NBS20	2.9608	1.0277	4.8332	0.212	$\Omega_6 > \Omega_2 > \Omega_4$	Present work
NBS25	2.2733	0.9155	3.8884	0.235	$\Omega_6 > \Omega_2 > \Omega_4$	Present work
SBNACZ	4.71	4.54	5.05	0.899	$\Omega_6 > \Omega_2 > \Omega_4$	[35]
BPN70	3.523	2.984	5.480	0.544	$\Omega_6 > \Omega_2 > \Omega_4$	[36]
CS-TCP	4.80	3.20	5.15	0.621	$\Omega_6 > \Omega_2 > \Omega_4$	[37]
40CaO-60SiO_2	4.26	4.06	4.71	0.861	$\Omega_6 > \Omega_2 > \Omega_4$	[38]
40BaO-60SiO_2	3.82	3.45	3.93	0.877	$\Omega_6 > \Omega_2 > \Omega_4$	[38]

more asymmetry, high covalency, and maximum rigidity as compared with the other Nd^{3+} doped NBS glasses.

Hypersensitive transition for Nd^{3+} doped NBS glasses is $^4I_{9/2} \rightarrow {}^4G_{5/2}$ situated around 582 nm in Fig. 5. This transition is entirely influenced by the RE ion-ligand surrounding and obeys the selection rule $\Delta S = 0$, $\Delta L \leq 2$ and $\Delta J \leq 2$. Along with this, the $^4I_{9/2} \rightarrow {}^4G_{5/2}$ transition possess maximum values for oscillator strengths and matrix elements $\|U^2\|^2$, showing an association with hypersensitivity and Ω_2 parameter (both are directly proportional). Ω_4 and Ω_6 help in calculating the radiative analysis like stimulated emission cross section, transition probability and branching ratio for the active ions. Ω_4 and Ω_6 are quite impactful in considering the neodymium emission intensity. For the present case, $^4F_{3/2} \rightarrow {}^4I_{9/2}$ transition is dependent upon Ω_4 while Ω_6 is accountable for $^4F_{3/2} \rightarrow {}^4I_{11/2}$ transition. Spectroscopic quality factor (χ), a ratio between Ω_4 and Ω_6, thats helps in recognizing the path way for the excited metastable state $^4F_{3/2}$ to decay to ground state. Smaller the value of χ, better will be the probability for lasing in NIR corresponding to $^4F_{3/2} \rightarrow {}^4I_{11/2}$ transition. According to relation between χ and NIR transitions ($^4F_{3/2} \rightarrow {}^4I_{9/2}$ and $^4I_{11/2}$), if its values are less than 1 then $^4F_{3/2} \rightarrow {}^4I_{11/2}$ transition has higher efficiency and is better for lasing. While if its values are more than one then, $^4F_{3/2} \rightarrow {}^4I_{11/2}$ transition efficiency is reduced and $^4F_{3/2} \rightarrow {}^4I_{9/2}$ transition efficiency is increased [42]. For the present case study, NBS10 possess minimum value of χ as 0.168 (however, usual reported values are in the range 0.22–1.5) and is shown in Table 2 [43].

3.4 Emission and radiative characteristics

Photoluminescene excitation spectra for 1 mol% (NBS10) Nd^{3+} doped NBS glass at 1068 nm emission wavelength is shown in Fig. 6. Eleven bands arising from $^4I_{9/2} \rightarrow {}^2I_{11/2}$, $^4D_{3/2}$, $^2P_{1/2}$, $^2K_{15/2}$, ($^4G_{9/2}$, $^2K_{13/2}$), ($^4G_{7/2}$, $^4G_{5/2}$), $^2H_{11/2}$, $^4F_{9/2}$, ($^4S_{3/2}$, $^4F_{7/2}$), $^2H_{9/2}$ and $^4F_{5/2}$ which are centered around 293, 358, 431, 475, 526, 585, 627, 683, 738, 800 and 825 nm in UV–vis–NIR range can be seen. Among all the transitions, 585 nm was the most intense peaks observed. Therefore, the emission spectra of all the prepared glass samples were recorded at this excitation wavelength. Figure 7 shows the emission spectra with three peaks in NIR range, arising from the transitions $^4F_{3/2} \rightarrow {}^4I_{9/2}$, $^4I_{11/2}$ and $^4I_{13/2}$ centered around 910, 1068 and 1339 nm respectively. Among these bands, the most intense one is at 1068 nm and so, is best suited for laser transition. In the inset diagram of Fig. 7 the variation of intensity for $^4F_{3/2} \rightarrow {}^4I_{11/2}$ transition with the concentration of Nd^{3+} ions as shown in the form of bar graphs. The observed intensity of $^4F_{3/2} \rightarrow {}^4I_{11/2}$ transition increases till 1 mol% of the RE ion beyond which, the intensity of the band decreases. This decrement is ascribed due to increased interaction among Nd^{3+}—Nd^{3+} ions and also among Nd^{3+}-host defects, resulting in the cross-relaxation process in the effective ion centres through concentration

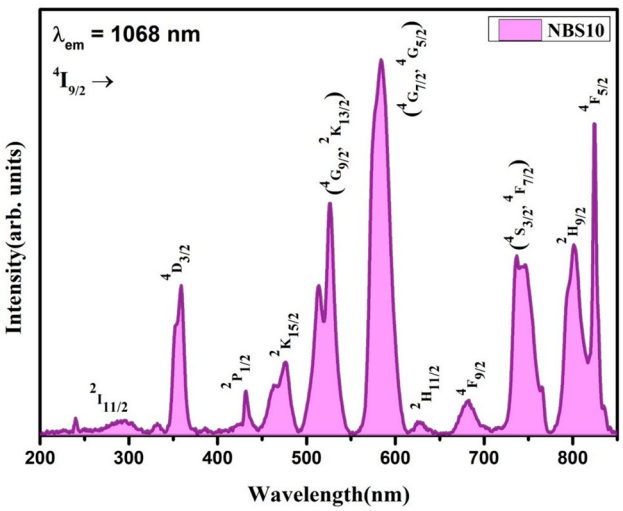

Fig. 6 Excitation spectra of Nd^{3+} ions in NBS10 glass monitored at 1068 nm emission

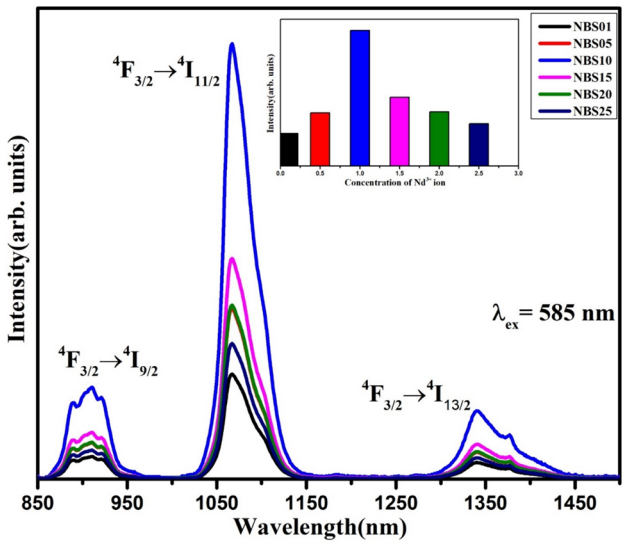

Fig. 7 Emission spectra of Nd^{3+} ions in NBS glasses under 585 nm excitation (*Inset* Variation of $^4F_{3/2}\rightarrow{}^4I_{11/2}$ transition with the concentration of Nd^{3+} ions)

quenching. Figure 8 depicts the diagram for energy level transitions of the Nd^{3+} ions in the NBS glasses emphasizing upon the excitation, emission and cross- relaxation processes. As the Nd^{3+} ions are excited from $^4I_{9/2}$ ground state to $^4F_{5/2}$ excited state, they decay to a metastable state $^4F_{3/2}$ via a non-radiative decay. This $^4F_{3/2}$ level gets strongly populated by Nd^{3+} ions resulting in three radiative transitions: $^4F_{3/2}\rightarrow{}^4I_{9/2}$, $^4I_{11/2}$ and $^4I_{13/2}$. The transition corresponding to $^4I_{11/2}$ is most intense. When the Nd^{3+} ions content is increased in the host glass system, it leads to reduction in the separation between Nd^{3+} ions resulting in increased cross- relaxation mechanism among the Nd^{3+} ions. These processes cumulatively depopulate the Nd^{3+} ions situated at $^4F_{3/2}$ energy level. Cross relaxation channels involved in the process is $^4F_{3/2}+{}^4I_{9/2}\rightarrow{}^4I_{15/2}+{}^4I_{15/2}$ result in loss of energy through non-radiative mechanism. The non radiative energy transfer can occur by either exchange interaction or multipolar interaction. The kind of inter-ionic interaction between the dopant ions can be accessed via Dexter Theory. The interactions can be grouped as dipole–dipole (d–d), dipole–quadrupole (d–q) and quadrupole—quadrupole (q–q). Based upon the relation between emission intensity and concentration of the activator ions, a graph can be plotted using the following relation [16]:

$$\log\frac{I}{c}=\log f-\frac{s\log(c)}{d} \tag{6}$$

Here I, c, f and d are emission intensity, concentration of activator ions, a constant which is independent of activator ions concentration and dimension of the compound (=3) respectively. Interaction between the closest neighbouring ions is predicted by s, where s = 6, 8 and 10 for d-d, d-q and q-q interaction respectively [16]. The plot between log (I/c) and log (c) is presented in Fig. 9 which shows the value of slope (s/d) to be 1.86, hence the calculated data for s = 1.86 *3 = 5.6. Here the obtained data for s is approximately equal to 6 indicating towards dipole–dipole interaction among the activator ions. Hence in the NBS glasses, dipole–dipole interaction is responsible for non-radiative energy transfer among Nd^{3+} ions. Moreover, this non radiative energy transfer leads to the concentration quenching effect in the emission spectra.

The radiative parameters like transition probability (A_R), total transition probability (A_T), radiative lifetime (τ_R) and branching ratio (β_R) corresponding to $^4F_{3/2}\rightarrow{}^4I_{9/2}$, $^4I_{11/2}$ and $^4I_{13/2}$ transitions for Nd^{3+} ions doped NBS glasses with the help of relations provided in literature were also calculated [44] and are represented in Table 3.

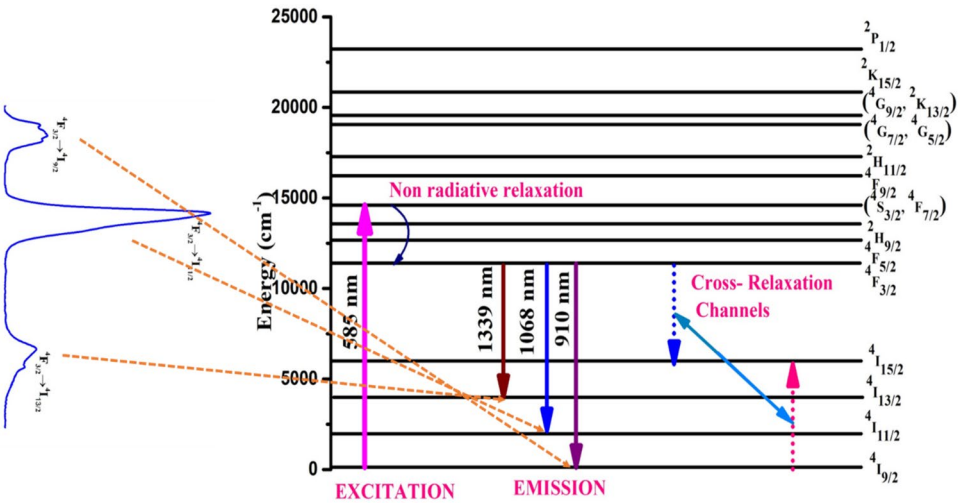

Fig. 8 Partial energy level diagram showing excitation, emission and cross-relaxation mechanism for Nd^{3+} ions in NBS glasses

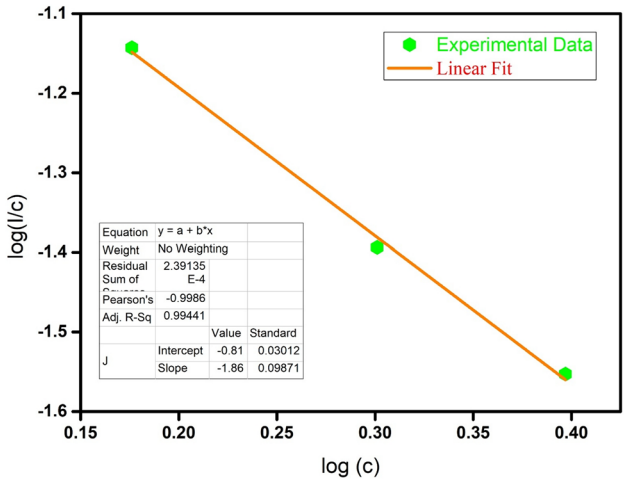

Fig. 9 Plot of log(I/c) v/s log(c) of Nd^{3+} ions in NBS glasses

From the data represented in Table 3, we can observe that the values of branching ratio (β_R) for NBS10 glass are maximum among all prepared Nd^{3+} doped NBS glasses corresponding to $^4F_{3/2} \rightarrow {}^4I_{11/2}$ transition. The values for total radiative transition probability increase upto 1 mol% of Nd^{3+} ions and then decrease upon further increment of the RE ions concentration. The total radiative transition probability for $^4F_{3/2} \rightarrow {}^4I_{11/2}$ is highest which is the most intense peaks. The fluorescence branching ratio is an important parameter in identifying the intensity for laser transition ascribed to electric dipole transitions of various excited and lower energy levels. If the value of β_R is ≥ 0.5 then it is very well suited for the lasing job. In the present study the value of β_R is above 0.5 for $^4F_{3/2} \rightarrow {}^4I_{11/2}$ energy level for all Nd^{3+} ions doped NBS making it as possible candidate for the lasing field applications. For further analyzing the utility as an appropriate lasing host, stimulated emission cross-section (σ_{se}) of the glass should be of high value. The value of stimulated emission cross-section suggests the behavior of energy extraction from optical material and is evaluated with the help of relation [1, 11]:

$$\sigma_{se} = \left[\frac{\lambda_p^4}{8\pi c n^2 \Delta\lambda_p}\right] A_R \tag{7}$$

where, the λ_p and $\Delta\lambda_p$ represent the wavelength corresponding to most intense band and linewidth (FWHM). Table 4 shows all the calculated values for stimulated emission cross-sections (σ_{se}), emission peak wavelength (λ_P), line widths ($\Delta\lambda_P$), gain band width ($\sigma_{se} \times \Delta\lambda_P$) and optical gain parameter ($\sigma_{se} \times \tau_R$) parameters for the emission transitions for Nd^{3+} ions in NBS glasses. The value of stimulated emission cross-section for NBS10 glass is maximum, making it superior host for lasing and optical fiber amplifier applications.

3.5 Decay spectral examination

Figure 10 shows the fluorescence decay curves for the Nd^{3+} ions in NBS glasses at 1068 nm emission wavelength for $^4F_{3/2} \rightarrow {}^4I_{11/2}$ transition under 585 nm excitation. The measured decay curves for the Nd^{3+} doped NBS glasses show single exponential fit behavior for all concentrations. The experimental decay time (τ_{exp}) for the Nd^{3+} doped NBS

Table 3 Transition probability (A_R) (s^{-1}), measured and experimental branching ratio (β_{exp} *and* β_R), total transition probability (A_T) (s^{-1}) and radiative lifetime (τ_R) (μs) for the observed emission transitions of Nd^{3+} ions in NBS glasses

Sample name	Transition	A_R	A_T	β_R	β_{exp}	τ_R
NBS01	$^4F_{3/2} \rightarrow {}^4I_{9/2}$	3468.18	13,736.8	0.2525	0.1653	72
	$^4F_{3/2} \rightarrow {}^4I_{11/2}$	8203.46		0.5972	0.6704	
	$^4F_{3/2} \rightarrow {}^4I_{13/2}$	1967.83		0.1433	0.1609	
NBS05	$^4F_{3/2} \rightarrow {}^4I_{9/2}$	3862.95	15,042.4	0.2568	0.1640	66
	$^4F_{3/2} \rightarrow {}^4I_{11/2}$	8938.47		0.5942	0.6680	
	$^4F_{3/2} \rightarrow {}^4I_{13/2}$	2135.44		0.142	0.1623	
NBS10	$^4F_{3/2} \rightarrow {}^4I_{9/2}$	4297.01	18,627.7	0.2307	0.1621	53
	$^4F_{3/2} \rightarrow {}^4I_{11/2}$	11,403.2		0.6122	0.6736	
	$^4F_{3/2} \rightarrow {}^4I_{13/2}$	2789.59		0.1498	0.1636	
NBS15	$^4F_{3/2} \rightarrow {}^4I_{9/2}$	3378.27	13,670.5	0.2471	0.1615	73
	$^4F_{3/2} \rightarrow {}^4I_{11/2}$	8214.18		0.6009	0.6743	
	$^4F_{3/2} \rightarrow {}^4I_{13/2}$	1980.17		0.1448	0.1615	
NBS20	$^4F_{3/2} \rightarrow {}^4I_{9/2}$	2967.57	12,024.9	0.2468	0.1617	83
	$^4F_{3/2} \rightarrow {}^4I_{11/2}$	7228.14		0.6011	0.6710	
	$^4F_{3/2} \rightarrow {}^4I_{13/2}$	1743		0.1449	0.1602	
NBS25	$^4F_{3/2} \rightarrow {}^4I_{9/2}$	2632.92	10,308.6	0.2554	0.1654	97
	$^4F_{3/2} \rightarrow {}^4I_{11/2}$	6135.38		0.5952	0.6710	
	$^4F_{3/2} \rightarrow {}^4I_{13/2}$	1467.7		0.1424	0.1559	

Table 4 Emission peak wavelength (λ_P) (nm), linewidths ($\Delta\lambda_P$) (nm), stimulated emission cross-sections (σ_{se}) (cm^2), gain band width ($\sigma_{se} \times \Delta\lambda_P$) ($cm^3$) and optical gain parameter ($\sigma_{se} \times \tau_R$) ($cm^2$ s) parameters for the emission transitions for Nd^{3+} ions in NBS glasses

Spectral parameters	NBS01	NBS05	NBS10	NBS15	NBS20	NBS25
$\lambda_P = 910$ nm ($^4F_{3/2} \rightarrow {}^4I_{9/2}$)						
Δλp	49.217	49.133	49.106	49.019	49.0	49.098
$\sigma_{se}(\times 10^{-22})$	109.491	117.266	126.388	97.204	82.153	71.086
$\sigma_{se} \times \Delta\lambda_P(\times 10^{-28})$	538.884	576.169	620.645	476.487	402.555	349.027
$\sigma_{se} \times \tau_R(\times 10^{-25})$	7.883	7.739	6.698	7.095	6.818	6.895
$\lambda_P = 1068$ nm ($^4F_{3/2} \rightarrow {}^4I_{11/2}$)						
Δλp	37.825	37.803	37.905	37.816	37.787	37.760
$\sigma_{se}(\times 10^{-22})$	639.333	669.081	824.368	581.245	492.292	408.644
$\sigma_{se} \times \Delta\lambda_P(\times 10^{-28})$	2418.302	2529.376	3124.806	2198.067	1860.249	1543.061
$\sigma_{se} \times \tau_R(\times 10^{-25})$	46.032	44.159	43.691	42.430	40.860	39.638
$\lambda_P = 1339$ nm ($^4F_{3/2} \rightarrow {}^4I_{13/2}$)						
Δλp	57.410	57.465	57.643	57.396	57.371	57.088
$\sigma_{se}(\times 10^{-22})$	249.660	259.815	327.658	228.103	193.188	159.760
$\sigma_{se} \times \Delta\lambda_P(\times 10^{-28})$	1433.304	1493.052	1888.749	1309.232	1108.356	912.044
$\sigma_{se} \times \tau_R(\times 10^{-25})$	17.975	17.147	17.365	16.651	16.034	15.496

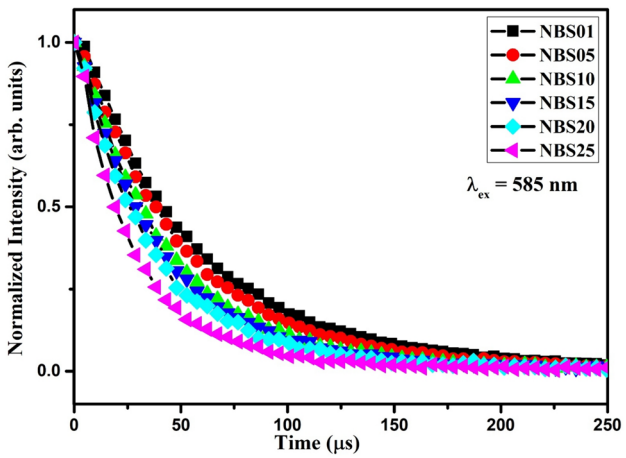

Fig. 10 Decay profiles of Nd^{3+} ions in NBS glasses for $^4F_{3/2} \rightarrow {}^4I_{11/2}$ transition under 585 nm excitation

Table 5 Experimental lifetime (τ_{exp}) (μs), radiative lifetime (τ_R) (μs), quantum efficiency (η), and non-radiative decay rates (W_{NR}) (s^{-1}) for Nd^{3+} ions in NBS glasses

Name of sample	τ_{exp}	τ_R	η (%)	W_{NR}
NBS01	56	72	77.7	3968
NBS05	51	66	77.2	4456
NBS10	44	53	83	3859
NBS15	41	73	56.1	10,691
NBS20	36	83	43.3	15,729
NBS25	28	97	28.8	25,405

glasses are calculated initially by applying e-folding time of the intensity for decay curves and with the help of equation provided in literature which are shown in Table 5 [8, 11, 22]. The values of τ_{exp} are found to be decreasing with increment in concentration of Nd^{3+} ions for NBS glasses which may be attributed to concentration quenching effect among the Nd^{3+} ions. The τ_{exp} values are also lower than the corresponding τ_R obtained via J–O theory, which may be ascribed due to specific the non-radiative decay mechanism (W_{NR}). Quantum efficiency (η), which is the ratio between emitted and absorbed light intensity, is an important parameter that describes the utility of the material for lasing applications. Higher the value of quantum efficiency, better will be the lasing properties of studied glass matrix. Following equations are used to determine the values of η and W_{NR} given in literature and are shown in Table 5 [8, 11]:

$$\eta = \frac{\tau_{exp}}{\tau_R} x100\% \tag{8}$$

$$W_{NR} = \left(\frac{1}{\tau_{exp}} - \frac{1}{\tau_R}\right) \tag{9}$$

From the obtained values we can see that the highest quantum efficiency and lowest non radiative decay rate is for 1 mol% of Nd^{3+} ions doped NBS glasses, which further ascertains its suitability for NIR laser emission at 1068 nm [45, 46].

The values of important parameters, such as stimulated emission cross-section, gain band width, optical gain, experiment decay time, quantum efficiency and non-radiative decay rate, of NBS glass are compared to other Nd^{3+}-doped glasses and are shown in Table 6, along with the other reported glasses doped with Nd^{3+} ions. The measured values for optimized NBS10 glasses are maximum from all the other prepared glass as well as other

Table 6 Stimulated emission cross-sections ($\sigma_{se}\times10^{-22}$) ($cm^2$), gain band width ($\sigma_{se}\times\Delta\lambda_P$) ($\times10^{-28}$) ($cm^3$), optical gain parameter ($\sigma_{se}\times\tau_R$) ($\times10^{-25}$) (cm^2 s), experimental lifetime (τ_{exp}) (μs), radiative lifetime (τ_R) (μs), quantum efficiency (η), and non-radiative decay rates (W_{NR}) (s^{-1}) for ($^4F_{3/2}\rightarrow{}^4I_{11/2}$) transition of Nd^{3+} ions in NBS glasses along with other reported values

Name of sample	$\sigma_{se}(\times10^{-22})$	$\sigma_{se}\times\Delta\lambda_P(\times10^{-28})$	$\sigma_{se}\times\tau_R(\times10^{-25})$	τ_{exp}	η (%)	W_{NR}
NBS01	639.333	2418.302	46.032	56	77.7	3968
NBS05	669.081	2529.376	44.159	51	77.2	4456
NBS10	824.368	3124.806	43.691	44	83	3859
NBS15	581.245	2198.067	42.43	41	56.1	10,691
NBS20	492.292	1860.249	40.86	36	43.3	15,729
NBS25	408.644	1543.061	39.638	28	28.8	25,405
LiPbAlBNd [47]	300	1330	4.41	113	77.1	2046
TTNW0 [48]	367	1056.9	-	133	66	-
LTTNd10 [49]	4750	1980	394	68	82	2657

reported values, which marks towards more suitability in various lasing applications.

4 Conclusions

Nd^{3+}doped NBS glasses were prepared via a melt quench technique. The X-ray diffraction pattern shows the amorphous behavior of the undoped glass. The Thermo-gravimetric analysis shows stability of the glass. A thorough spectroscopic analysis of the samples was done via characterization techniques like UV–VIS-NIR absorption, photoluminescence excitation and emission and time decay measurements. Judd–Ofelt analysis was conducted and three intensity parameters Ω_2, Ω_4 and Ω_6 were obtained for all the prepared glass samples from the absorption data. Various important radiative parameters were calculated to help assess the suitability of the glasses in lasing applications. Emission of the Nd^{3+} doped NBS glasses was found in NIR range with three prominent transitions corresponding to $^4F_{3/2}\rightarrow{}^4I_{9/2}$, $^4I_{11/2}$ and $^4I_{13/2}$, wherein $^4F_{3/2}\rightarrow{}^4I_{11/2}$ transition centered at 1068 nm had the maximum intensity. This transition possesses the maximum value of spectroscopic quality factor, branching ratio, stimulated emission cross section and quantum efficiency for the optimized glass (NBS10). Interaction among the activator ions was predicted to be of dipole–dipole nature by utilizing the Dexter theory. The decay curves for NBS glasses show single exponential for all concentrations. The aforementioned results are encouraging enough to ascertain that the 1 mol% of Nd^{3+} ions doped NBS glass is ideal for laser and fiber amplifier applications.

Acknowledgements One of the authors Dr. Yasha Tayal is grateful to the management of ABES Engineering College Ghaziabad Uttar Pradesh for providing a conducive work and research environment. She also acknowledges Prof. A.S. Rao for his impeccable research guidance that helped in achieving the desired results in this work.

Author contribution Y. Tayal: Conceptualization, Formal analysis, writing & editing, Investigation. R.A. Talewar: Formal analysis, review. Sk. Mahamuda: Formal analysis. K. Maheshwari: Formal analysis. S. Kumari: Formal analysis. R. Pilania: Formal analysis. M. Kumar: Formal analysis. A. Prasad: Formal analysis, review. A.S. Rao: Supervision, Writing-review & editing.

Data availability The data that support the findings of this study are available on request from the corresponding author Dr. Yasha Tayal. The data are not publicly available due to restrictions, e.g. their containing information that could compromise the privacy of research participants.

Declarations

Conflict of interest The authors declare that they have no known competing financial interests or personal relationships that could have appeared to influence the work reported in this paper.

References

1. F. Zaman, G. Rooh, N. Srisittipokakun, S. Ruengsri, H.J. Kim, J. Kaewkhao, J. Non-Cryst, Solids **452**, 307 (2016)
2. C.M. da Silva Jr, L.A. Bueno, A.S. Gouveia-Neto, J. Non- Cryst. Solids **410**, 151 (2015)
3. M.D. Dramićanin, Methods Appl. Fluoresc. **4**, 042001 (2016)
4. C.X. Liu, X.L. Shen, H.T. Guo, W.N. Li, W. Wei, Optik **131**, 132 (2017)
5. N.K. Goel, G. Pickrell, R. Stolen, Opt. Fiber Technol. **20**, 325 (2014)
6. F. Elan, E.L. Falcão-Filho, M.E. Camilo, J.A.M. Garcia, L.R.P. Kassab, C. de Araújo, Opt. Mater. **60**, 313 (2016)
7. S. Mohan, K.S. Thind, Opt. Mater. **57**, 134 (2016)
8. C.R. Kesavulu, H.J. Kim, S.W. Lee, J. Kaewkhao, N. Wantana, E. Kaewnuam, S. Kothan, S. Kaewjaeng, J. Alloys Compd. **695**, 590 (2017)
9. L.R.P. Kassab, D.M. Silva, J.A.M. Garcia, D.S. da Silva, C.B. de Araújo, Opt. Mater. **60**, 25 (2016)
10. H.K. Dan, D.C. Zhou, Z.W. Yang, Z.G. Song, X. Yu, J.B. Qiu, J. Non-Cryst, Solids **414**, 21 (2015)
11. T.F. Xue, L.Y. Zhang, J.J. Hu, M.S. Liao, L.L. Hu, Opt. Mater. **47**, 24 (2015)

12. A. Pandey, S. Som, V. Kumar, V. Kumar, K. Kumar, V. KumarRai, H.C. Swart, Sensors Actuators B **202**, 1305 (2014)
13. D.D. Ramteke, R.E. Kroon, H.C. Swart, J. Non-Cryst, Solids **457**, 157 (2017)
14. L.Y. Zhang, B.H. Yang, L.L. Hu, J. Quant. Spectrosc. Radiat. Transf. **147**, 47 (2014)
15. S.M. Lima, J.A. Sampaio, T. Catunda, A.S.S. de Camargo, L.A.O. Nunes, M.L. Baesso, D.W. Hewak, J. Non-Cryst. Solids **284**, 274 (2001)
16. Y. Tayal, A.S. Rao, Opt. Mat. **107**, 110070 (2020)
17. J.A. Savage, Mater. Sci. Rep. **2**, 99 (1987)
18. H. Yamasaki, K. Minato, D. Nezaki, T. Okamoto, A. Kawamoto, M. Takata, Solid State Ionics **172**, 349 (2004)
19. Y. Tayal, A.S. Rao, Opt. Mat. **117**, 111112 (2021)
20. Y.I. Alivov, D.C. Look, B.M. Ataev, M.V. Chukichev, V.V. Mamedov, V.I. Zineko, Y.A. Agafonov, A.N. Pustovit, Solid State Electron. **48**, 2343 (2004)
21. B.L. Zhu, C.S. Xie, D.W. Zeng, W.L. Song, A.H. Wang, Mater. Chem. Phys. **89**, 148 (2005)
22. Y. Tayal, A.S. Rao, S. Kaur, Solid State Sci. **125**, 106834 (2022)
23. X.F. Wang, Q. Liu, Y.Y. Bu, C.S. Liu, T. Liu, X.H. Yan, RSC Adv. **5**, 86219 (2015)
24. S. Rai, A.L. Fanai, J. Lumin. **170**, 325 (2016)
25. C. Tian, X. Chen, Y. Shuibao, Solid State Sci. **48**, 171 (2015)
26. B. Klimesz, G. Dominiak-Dzik, P. Solarz, M. Zelechower, W. RybaRomanowski, J. Alloys Compd. **403**, 76 (2005)
27. S. Mohan, K.S. Thind, G. Sharma, L. Gerward, Spectro chim. Acta Part A **70**, 1173 (2008)
28. Y. Tayal, R.A. Talewar, S.K. Mahamuda, A. Prasad, K. Maheshwari, M. Kumar, A.S. Rao, Opt. Mater. **142**, 114049 (2023)
29. K. Linganna, R. Narro-García, H. Desirena, E. De la Rosa, Ch. Basavapoornima, V. Venkatramu, C.K. Jayasankar, J. Alloys Compd. **684**, 322 (2016)
30. W.T. Carnall, P.R. Fields, K. Rajnak, J. Chem. Phys. **49**, 4424–4442 (1968)
31. G.S. Ofelt, J. Chem. Phys. **37**, 511 (1962)
32. P. Babu, C.K. Jayasankar, Opt. Mater. **15**, 65 (2000)
33. R. Praveena, V. Venkatramu, P. Babu, C.K. Jayasankar, Phys. B **403**, 3527 (2008)
34. S. Tanabe, T. Ohyagi, N. Soga, T. Hanada, Phys. Rev. B **46**, 3305 (1992)
35. T. Suzuki, H. Nasu, M. Hughes, S. Mizuno, K. Hasegawa, H. Ito, Y. Ohishi, J. Non Cryst. Solids **356**, 2344 (2010)
36. M.B. Saisudha, J. Ramakrishna, Phys. Rev. B **53**, 6186 (1996)
37. J.A. Pardo, J.I. Pena, R.I. Merino, R. Cases, A. Larrea, V.M. Orera, J. Non Cryst. Solids **298**, 23 (2002)
38. H. Takebe, K. Morinaga, T. Izumitami, J. Non-Cryst, Solids **178**, 58 (1994)
39. W.T. Carnall, H. Crosswhite, H.M. Crosswhite, Technical report, Argonne National. Laboratory (1997). https://doi.org/10.2172/6417825
40. D.D. Ramteke, A. Balakrishna, V. Kumar, H.C. Swart, Opt. Mater. **64**, 171 (2017)
41. C.R. Kesavulu, H.J. Kim, S.W. Lee, J. Kaewkhao, N. Wantana, S. Kothan, S. Kaewjaeng, J. Alloys Compd. **683**, 590 (2016)
42. J. Azevedo, J. Coelho, G. Hungerford, N.S. Hussain, Phys. B: Condens. Matter. **405**, 4696 (2010)
43. M. Ajroud, M. Haouari, H.B. Ouada, H. Maaref, A. Brenier, C. Garapon, J. Phys. Condens. Matter **12**, 3181 (2000)
44. R. Cases, M.A. Chamarro, R. Alcala, V.D. Rodriguez, J. Lumin. **48**, 509 (1991)
45. Q.L. Chen, H. Wang, Q.P. Chen, J. Non-Cryst, Solids **391**, 43 (2014)
46. D. Ramachari, L.R. Moorthy, C.K. Jayasankar, Opt. Mater. **36**, 823 (2014)
47. N. Deopa, A.S. Rao, M. Gupta, G.V. Prakash, Opt. Mater. **75**, 127–134 (2018)
48. H. Fares, I. Jlassi, S. Hraiech, H. Elhouichet, M. Ferid, J. Quant. Spectrosc. RA. **147**, 224–232 (2014)
49. M. Venkateswarlu, S.K. Mahamuda, K. Swapna, M.V.V.K.S. Prasad, A.S. Rao, A.M. Babu, S. Shakya, G.V. Prakash, Opt. Mater. **39**, 8–15 (2015)